J. Appl. Comput. Mech., 8(4) (2022) 1407-1421
DOI: 10.22055/jacm.2022.40366.3574

ISSN: 2383-4536
jacm.scu.ac.ir

Shahid Chamran University of Ahvaz

Journal of Applied and Computational Mechanics

Research Paper

Computational and Experimental Study of the Composite Material for the Centrifugal Pump Impellers Manufacturing

Madina Isametova[1], Rollan Nussipali[2], Dimitar Karaivanov[3], Zhastalap Abilikhair[4], Aysen Isametov[5]

[1] Department of Mechanical Engineering, Standardization, Certification and Metrology, Institute of Energy and Mechanical Engineering, Satbayev University, Satpaev Street 22, Almaty, KZ-050000, Kazakhstan, Email: isametova69@mail.ru

[2] Department of Mechanical Engineering, Standardization, Certification and Metrology, Institute of Energy and Mechanical Engineering, Satbayev University, Satpaev Street 22, Almaty, KZ-050000, Kazakhstan, Email: rollan_n@mail.ru

[3] Department of Applied Mechanics, University of Chemical Technology and Metallurgy, 8 St Kliment Ohridski Blvd, Sofia, BG-1756, Bulgaria, Email: dipekabg@yahoo.com

[4] Department of Mechanical Engineering, Standardization, Certification and Metrology, Institute of Energy and Mechanical Engineering, Satbayev University, Satpaev Street 22, Almaty, KZ-050000, Kazakhstan, Email: jastalap81@mail.ru

[5] Department of Mechanical Engineering, Standardization, Certification and Metrology, Institute of Energy and Mechanical Engineering, Satbayev University, Satpaev Street 22, Almaty, KZ-050000, Kazakhstan, Email: eadevat627@mail.ru

Received March 27 2022; Revised May 12 2022; Accepted for publication May 15 2022.
Corresponding author: R. Nussipali (rollan_n@mail.ru)

Abstract. The mechanical properties of a polycarbonate matrix composite with glass fiber reinforcements used for the manufacture of a multistage centrifugal pump impeller are researched in this article. The material properties are modelled using DIGIMAT (The Material Modelling Platform) to determine the strain resistance of the composite with different proportions of reinforcements. The Tsai–Hill failure criterion is used to determine the strength in all cases. The results have been verified by physical testing to determine the influence of the shape and mass proportion of reinforcements on its mechanical properties. The strength of the manufactured part is correlated to technological factors using the MARC MENTAT solver, and the most and the least favorable combinations of these factors are determined.

Keywords: Impeller, polymer-composite materials, mechanical schematic, stress, strain.

1. Introduction

One of the global trends in technology is the gradual replacement of traditional materials with polymer composites. One of the areas of application of polymer-composite materials in engineering is the manufacturing of impellers for electrical submersible centrifugal pumps. Polymer-composite materials (PCM) are widely used due to their largely unique properties. The decisive factor in the rapid development of PCM production was determined to be in its competitiveness to traditional materials. Nowadays, PCMs are used in almost all engineering applications [1]. One of the actively developing areas has become the manufacture of pump impellers (PI) for electrical submersible centrifugal pumps (ESP2PCM materials make it possible to conduct a thorough optimization of the system based on pump weight reduction and increase in productivity taking to account the individual design constraints).

When considering the PCM, designers can also look forward to thermal, corrosion and oxidation resistance, thermal, acoustic, and electrical insulation through shorter manufacturing processes and reduced material waste and increased overall savings [2]. The automotive industry was the first industry to benefit from progressive replacement of metal to PCMs. A gradual decrease in the presence of ferrous metals (in the form of steel alloys, carbon steel, cast iron and wrought iron) and non-ferrous metals (primarily aluminum) in vehicle construction over the years has been reported [2].

The authors of [3, 4] distinguish the advantages of composite materials in their effect of reducing weight without affecting strength that is clearly demonstrated in the aviation industry. Multifunctional composite materials are intended to change the aviation industry approaches for the design and manufacture of load-bearing structures. The idea is that in the future, composite materials that are currently used only for load bearing applications should carry out additional duties as well. For example, a multifunctional material can be a load-bearing material with excellent thermal and electrical properties, providing improved structural resistance to lightning strikes and high EMI protection [3]. Additionally, a large review of research in the field of polymers and composites for manufacturing centrifugal pump impeller wheels has been conducted in [4, 5].

Published online: May 26 2022

In a polymer matrix composite, the mechanical properties of the materials are planned to be improved by using the fiber as a reinforcement of the polymer matrix. According to the type of matrix and reinforcement, composites can be classified into different categories. In general, reinforcing fiber can be categorized as inorganic, glass, and carbon fibers [6], while composite materials reinforced with either glass fibers (GF) or carbon fibers (CF) have been included in more than 90% of studies [7]. Thermoplastic [8] or thermosetting [9] polymers were used as polymer matrices for the manufacture of impellers. It should be said though that while composites have excellent dimensional stability under load, this ability makes them unsuitable for high-viscosity applications, where deformable rotors are needed in positive displacement type pumps [10].

Composites made of a polymer matrix reinforced with glass fiber are commonly used in the manufacture of impellers [11]. In general, fiberglass is an inorganic non-metallic material. The properties of these fibers include heat resistance, high tensile strength, and excellent chemical stability [12]. The glass fiber composition consists of SiO_2, Al_2O_3, TiO_2, B_2O_3, CaO, MgO, Na_2O, K_2O, and Fe_2O_3.

The diversity in fiber composition results in different mechanical properties, placing the average value of Young's modulus in the range from 51.7 to 86.9 [12]. Nayack and Ray [13] carried out a study of the residual mechanical properties of polymer composites reinforced with glass fiber. Improving the wear-resistant properties of glass fiber reinforced composites is another important factor that has attracted the attention of many studies [14]. Ozturk et al. [15] conducted an analysis of the erosive wear behavior of epoxy resin where glass fiber reinforcement has been evaluated with respect to various parameters such as different impact angles (20° to 90°), impact velocity in the range of 70-200 mm/s, impact time and extent of erosion. According to the results of the analysis, the highest erosion resistance was achieved for composite material consisting of 16 % weight SiO_2 (silica).

Maras et al. [16] carried out a study of an impeller consisting of 40 % weight fiberglass reinforced with PPS in an automotive water pump application. The rotational velocity has been set to 4500 rpm, and water and ethylene glycol have been chosen as the working fluids in the temperature range of 80-100°C. The maximum radial and tangential stresses determined by the pressing of the impeller have been calculated at 100 and 83.5 MPa respectively. Considering the physical and mechanical properties of glass reinforced PPS and the maximum impeller load, the material has been considered convenient for the case.

Another study considers comparison of organic Rankine cycle microturbines consisting of aluminum, ABS, and PEEK-G30. The impeller diameter has been chosen at 49 mm, the rotational velocity has been set to 36000 rpm, and R245fa selected as the working fluid. According to the study, in addition to the fact that PEEK-GF30 and ABS are convenient for mass production, the other benefits are low manufacturing costs, high chemical resistance and reduced rotational inertia. This minimizes imbalances, shaft fatigue and impeller case damage in the event of a failure. Additionally, simulation results have shown that PEEK-GF30 and ABS perform favorably in such conditions and present a good alternative to aluminum [17].

In [18], the authors studied the manufacture of fibrous composites and compared them with fiberglass and carbon fiber and explored the possibility of their use as structural materials for industrial purposes. The mechanical properties of the composite are determined by tensile testing of composite laminates (at various strain rates and temperatures), bending tests (at various strain rates) and impact tests. It is generally known that thermoplastic matrices have a high water absorption coefficient, therefore this article is aimed at researching the strength of polycarbonate matrix and GF based PCM.

The focus for increasing the economic efficiency of the use of ESP with PCM PI is on the reduction of the high cost of forming equipment due to the lack of market competition between manufacturers. The development and implementation of PCM recycling technology by equipment manufacturers would contribute to reduce the life cycle cost of its operation, as well as to reduce the environmental impact of used composite materials.

2. Impeller Geometry, Finite Element Mesh and Loading Conditions

The object of study is the impeller of a four-stage vertical centrifugal pump. For an impeller made of PM the creation of a precise geometry is of high importance for manufacturing by injection molding technology. The PUMP module written in the PYTHON language allows the creation of precise geometry. The input data for the design is given in Table 1. The blade coordinates are determined with an accuracy of 4 decimal places, which has an impact on the accuracy of the geometry of the impeller and the tooling for the technological process of molding.

Figure 1 shows the interface for computer-aided design of a blade profile developed in the PYTHON environment. The coordinates of the meridian profile of the wheel section and the curvature of the blade were imported into the CAD system. The impeller model is shown in Figure 2.

It is necessary to create an adequate computational mechanical schematic when the impeller model is being prepared for the simulation. There are many methods of calculating the forces acting on centrifugal multistage pump impellers covered in literature [19–22]. To verify the analytical calculations and determine the pump head and kinematic characteristics of a pump stage, the simulation and modeling of the flow was carried out in the Sflow system. The computational mechanical schematic for determining the forces acting on the centrifugal multistage pump impeller is shown in Figure 3.

Figure 4 shows a fluid flow simulation in the channels of the impeller performed using the SFlow software package, obtaining the values of the pressure (pump head) and flow velocity in the impeller.

According to the simulation results, the maximum pressure formed in the impeller channels reaches P = 73622.75 Pa, and the absolute velocity at the outlet of the impeller is w = 16.72 m/s.

The strength calculation of the impeller of a centrifugal pump includes the calculation of the blades in tension due to the action of centrifugal forces and the calculation of the load of fluid pressure on the front and rear sides of the impeller disc. The calculation of the blades under tension load implies determination of the stress caused by centrifugal force.

Table 1. Design input data.

Property	Designation	Unit	Value
Nominal pump volumetric flow	Q_H	m^3/h	15
Pump head	H_H	m	46
Rotational velocity	n_H	rpm	2850
Working fluid		Water	
Temperature	t	°C	20…40
Density	ρ	kg/m^3	1050

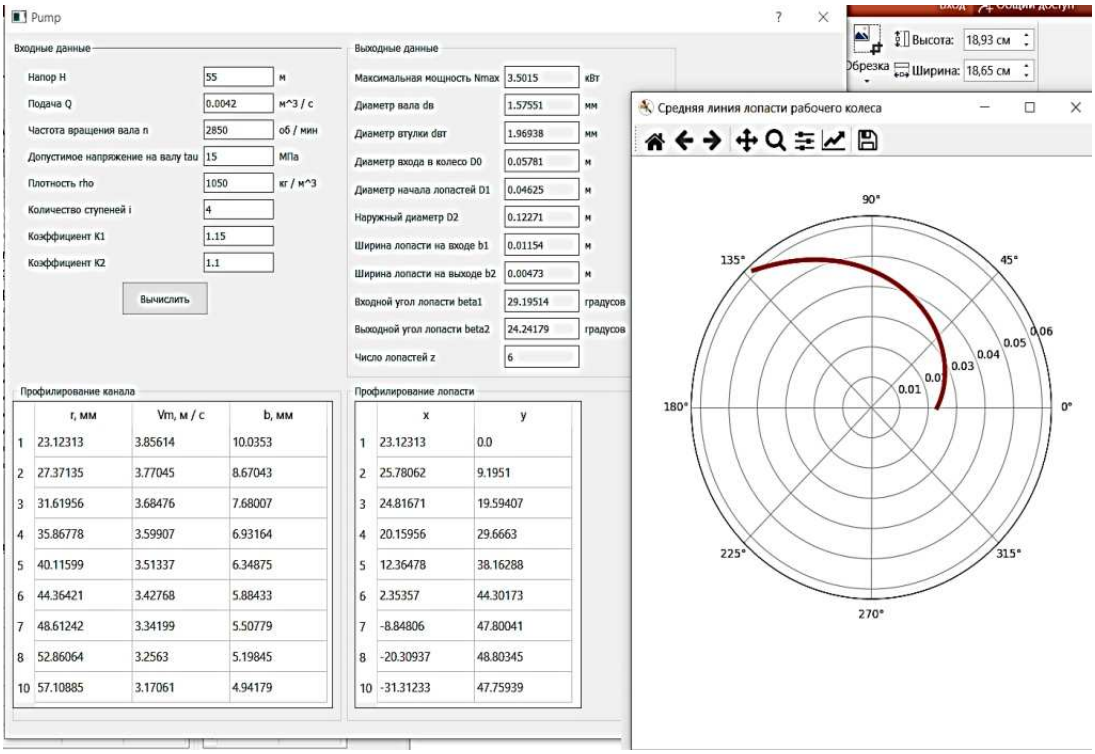

Fig. 1. Blade profile and meridian cross-section.

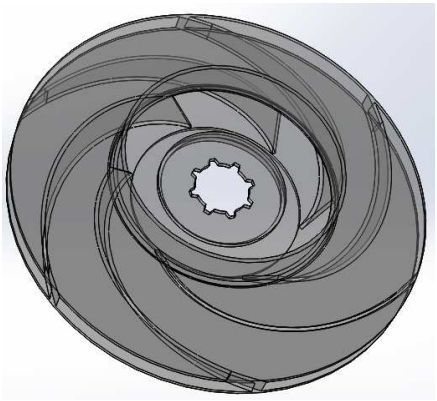

Fig. 2. 3D impeller model.

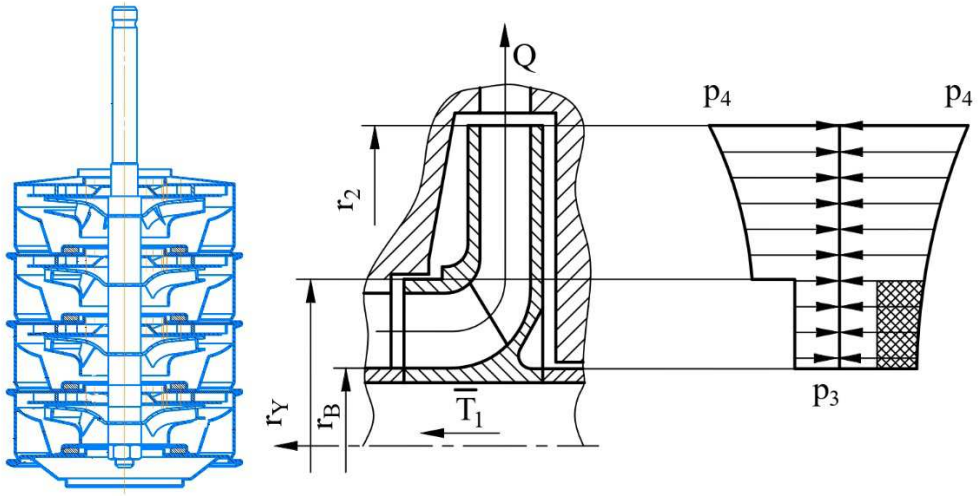

Fig. 3. Left: Pump cross-section. Right: Loading scheme with pressure balance on fourth stage pump impeller.

Table 2. Static impeller calculation data.

Property	Value
Pressure on impeller walls	0.072 MPa
Dead load on hinged elements	0.5 N
Young's modulus	$2{\cdot}10^5$ MPa
Poisson's ratio	0.3

For blades having a constant cross-sectional area, the centrifugal force is to be obtained by the following formula:

$$F_C = \rho \cdot \omega \cdot F \cdot (r_2 - r_B) \tag{1}$$

where r_2 and r_B are the outer and inner radius of the impeller. The results of the flow simulation data in the Sflow program have shown that the pressure on the impeller walls equals P = 0.072 MPa, and an analysis of the strength of the impeller was carried out. According to the calculation scheme given in [20] and the results obtained in the SFD module, the input data for the static calculation of the impeller is summarized in Table 2.

The results of the steel impeller calculation in the NASTRAN software package are shown in Figure 5. The density of the grid or the degree of refinement of the elements is one of the most important parameters for controlling the accuracy of the solution (the importance of type and shape of the chosen elements is high). In the ideal case of absence of singularities in the model (sharp corners, point loads and point restraints, etc.), a finer mesh, provides a more precise result. However, numerous elements in a fine mesh requires large amounts of computer RAM and computational time. This is especially valid for types of analysis where convergence requires multiple iterations per step, such as non-linear or transient analysis.

One of the methods of assessing the quality of the mesh (and the model as a whole) is the verification of the calculation results using experimental data or analytical solutions. Unfortunately, they are not always available to the user if they exist at all. Thus, other methods of quality assessment have found application in engineering practice. These include sequential mesh refinement, as well as interpolation for jumps in the obtained values.

The main and the most accurate method for assessing the quality of a mesh has been shown to be a successive reduction in the size of the elements until some significant result, such as, for example, the maximum stress in a certain zone, converges to a certain value (that is, with each iteration, the change in stress will be less than the specified permissible value) [24-25].

A study was carried out on a 3D model of an impeller fixed at the mounting position on the shaft. The stress concentration zone, obviously, is located at the edges of the blades and the mounting position of the impeller. The graph in Figure 5 shows the dependence of the maximum equivalent stress in the concentrator on the number of finite elements per unit area. It can be seen from the graph that an increase in the mesh density first leads to a sharp increase in the maximum stress, then the rate of increase slows down significantly and, as a result, the curve reaches an almost horizontal "shelf", where a large increase in the mesh density corresponds to relatively small change of the maximum stress value.

In this case the initial and terminal points of the area can be considered these with density of 1150 and 4500 elements per unit area. When the density increased for four times, the value of the stress increased only by 1.5%.

According to the calculation results (Fig. 6) σ_{max} equals to 66.4 MPa, displacement y equals to 0.00229 m, so considering the standard ultimate factor of safety for the impeller, the designed composite material should have an allowable tensile strength $\sigma_в$ equal to 150 MPa.

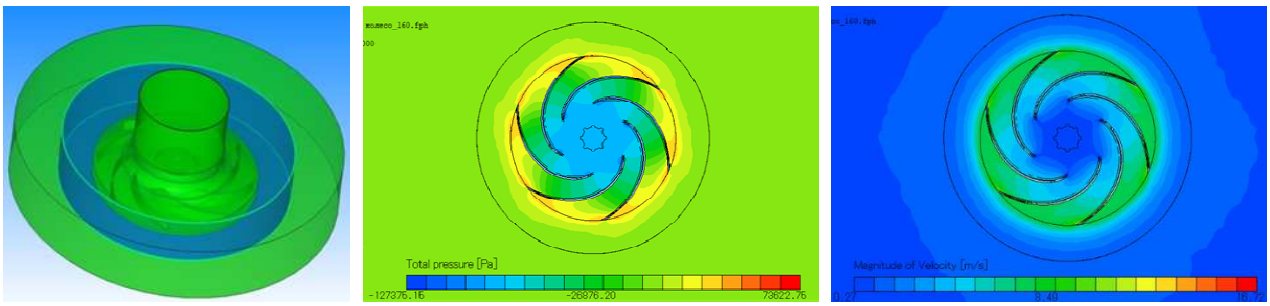

Fig. 4. Left: Impeller domain model. Center: Pressure distribution diagram. Right: velocity distribution diagram.

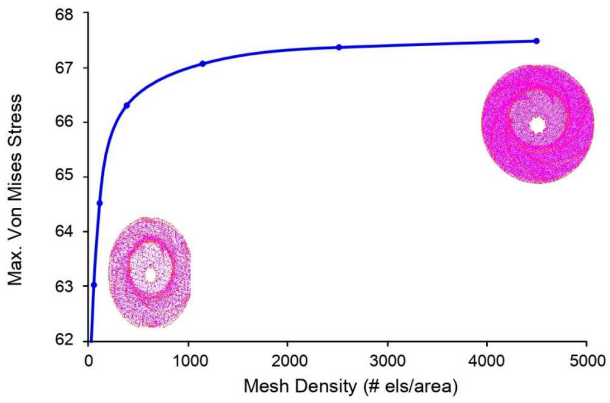

Fig. 5. Influence of mesh quality on stress values.

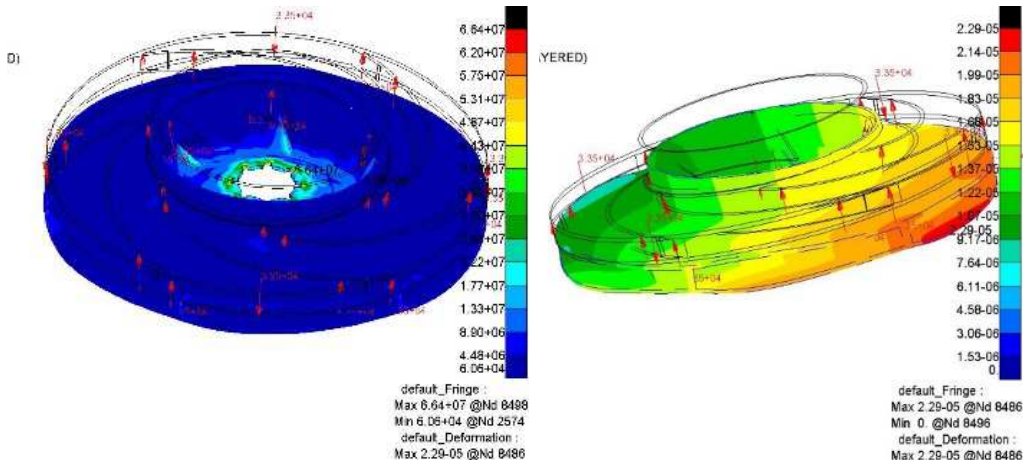

Fig. 6. Left: Stress-strain diagram in the horizontal section of the impeller. Right: Stress-strain diagram in the vertical cross section of the impeller.

3. Microscale Prediction of Composite Material Mechanical Properties

The properties of the designed composite material must meet the operating conditions of the part. The designed material with low water permeability must withstand a stress level of 150 MPa under load. Since the new composite material will be used to produce impellers of a multistage pump, the water absorption coefficients are 1-7% for polyamide and 0.36% for polycarbonate [26, 27]. Polycarbonate is chosen as the matrix material and fiberglass as reinforcing element.

The problem of replacing a steel impeller with a composite one can be solved in two ways: by choosing an existing material composition or designing a new material with the required properties. The MX module of the DIGIMAT automated system was used here as a reference book for existing brands of glass polymer compositions, as it contains data on more than 500 commercially available compositions. This database contains no data on no glass fiber reinforced polycarbonate matrix materials in the database, so further research must be performed.

3.1 Theoretical background

The basic theoretical approach for determining the mechanical characteristics of two-phase composites is based on the work of J. Eshelby. The modulus of elasticity (Young's modulus) for fibrous and dispersion-strengthened isotropic matrix composites is calculated according to the theories of Eshelby, Tandom and Weng, as well as the Maury-Tanaka theorem. Equations 2-7 are used to define five independent constants corresponding to Young's modulus, shear and bulk modulus and Poisson's ratio of the composite material [28, 29].

$$\frac{E_{11}}{E_m} = \frac{1}{1+\left(c_r\left(A_1+2\nu_m A_2\right)\right)/\left(A\right)} \tag{2}$$

$$\frac{E_{22}}{E_m} = \frac{E_{33}}{E_m} = \frac{1}{1+\left(c_r\left(-2\nu_m A_3+(1-\nu_m)A_4+(1+\nu_m)A_5 A\right)\right)/\left(2A\right)} \tag{3}$$

$$\frac{\mu_{12}}{\mu_m} = 1+\frac{c_r}{2c_m S_{1212}+\left(\mu_m\right)/\left(\mu_r-\mu_m\right)} \tag{4}$$

$$\frac{\mu_{23}}{\mu_m} = 1+\frac{c_r}{2c_m S_{2323}+\left(\mu_m\right)/\left(\mu_r-\mu_m\right)} \tag{5}$$

$$\frac{\kappa_{23}}{\kappa_m} = \frac{(1+\nu_m)(1-2\nu_m)}{1-\nu_m(1+2\nu_{12})+c_r\left(2(\nu_{12}-\nu_m)A_3+A_4\left(1-\nu_m(1+2\nu_{12})\right)\right)/A} \tag{6}$$

$$\upsilon_{12} = \frac{\upsilon_m A - c_r(A_3-\upsilon_m A_4)}{A+c_r(A_1+2\upsilon_m A_2)} \tag{7}$$

Expressions for the coefficients A_1, A_2, ... A, and the components of the Eshelby tensor, S_{igkl}, depending on the shape of the inclusions and the elastic characteristics of the phases, can be found in [27]. The modulus of elasticity introduced in this way provides effective values that determine the macroscopic elastic properties of the material.

The above theories allow us to determine the engineering constants for the designed PCM, so to predict the strength of the structure, it is necessary to use the equivalent stress criteria, as well as the Tsai-Hill criterion for transversely isotropic bodies (3D), using the setting of the first destroyed FPGF pseudo-grain [30,31] (Eq. 8):

$$\frac{1}{2}\left\{\left(\frac{1}{\sigma_{B11}^2}+\frac{1}{\sigma_{B22}^2}-\frac{1}{\sigma_{B33}^2}\right)\left(\sigma_{11}-\sigma_{22}\right)^2+\left(-\frac{1}{\sigma_{B11}^2}+\frac{1}{\sigma_{B22}^2}+\frac{1}{\sigma_{B33}^2}\right)\left(\sigma_{22}-\sigma_{33}\right)^2+\left(\frac{1}{\sigma_{B11}^2}-\frac{1}{\sigma_{B22}^2}+\frac{1}{\sigma_{B33}^2}\right)\left(\sigma_{11}-\sigma_{33}\right)^2\right\}+\frac{1}{\tau_{B12}^2}\tau_{B12}^2+\frac{1}{\tau_{B23}^2}\tau_{B23}^2+\frac{1}{\tau_{B13}^2}\tau_{B13}^2=1 \tag{8}$$

where σ_{ii} and τ_{ij} are the axial and shear components of the Cauchy stress tensor, and σ_{Bii} and τ_{Bij} – are the ultimate factor of safety along the corresponding directions.

Table 3. Input data for numerical simulation of composite material.

Parameter	Value
Polycarbonate modulus of elasticity	2360 MPa
Polycarbonate density	$1.14 \cdot 10^{-9}$ kg/mm^3
Polycarbonate lower yield strength	63 MPa
Polycarbonate hardness	95 HB
Glass modulus of elasticity	7200 MPa
Glass density	$7.8 \cdot 10^{-9}$ kg/mm^3
Poisson's ratio of glass	0.3

Table 4. Geometric parameters of chopped glass fiber reinforcements.

Fiber brand	Fiber diameter	Fiber length	Particle shape
ECS 11-4.5-560A	11 μm	4.5 mm	Fiber
ECS 13-3-552B	13 μm	3…6…12 mm	Fiber
CS 7938	50 μm	4.5 mm	Ellipsoid
CC	10 to 90 μm	-	Hollow glass spheres

3.2 Data for modeling composite material properties

The MSC Digimat MF module was used to implement the simulation on the microlevel approach. The input data is summarized in Table 3.

Papers published until now [32-37] deal with four main shapes of reinforcement particles such as sphere, parallelepiped (or needle-shaped particles), flake and fiber. For this experiment, fibers, ellipsoids, and spheres were selected as representative of elements in common usage (Fig. 7).

Nowadays, there are many companies supplying chopped glass fiber with various geometric properties. The geometric properties of the fiber grades used for numerical analysis are summarized in Table 4. The analysis was carried out with particles having aspect ratios k_r equal to 400, 20, and 1.

Data from the MX module was used to determine the optimal proportion of the reinforcement in the matrix, where the percentage of reinforcement in different compositions varies from 10% to 70%. Data on experiments [38] for determining the strength of composites, suggests that inclusion of reinforcement beyond 70% by weight results in brittle failure of the composite material. The optimal proportion of reinforcement was then determined by numerical simulation with 10%, 20%, 30%, 40%, 50%, and 60% of reinforcement.

4. Results of the Numerical Simulation of the Mechanical Material Properties of Composite Materials

The DIGIMAT composite modeling technology relies on micromechanical approaches to accurately predict the behavior of complex multi-component materials and allows bridging of the gap between composite material design, manufacturing process, and finite element analysis. DIGIMAT can simulate the characteristics of thermoplastics, thermosetting plastics, and composite materials with different matrices (polymeric, metallic, and rubber based). It is possible to consider the heterogeneity of the structure of materials associated with the technological processes of manufacturing composites, such as injection molding, laying out, and pressing [39,40]. The calculated characteristics of the materials will then be translated to an equivalent homogenous material, the properties of which can then be transferred to finite element software packages or DIGIMAT (Fig. 8).

4.1 Influence of the reinforcement shape factor on the mechanical properties of polycarbonate matrix composite materials

The results of the study of the influence of the aspect ratio of the reinforcement particles on the stress-strain curve of the material, is presented in Figure 9. The graphs presented in Figure 10 show a large spread in the values of the mechanical properties of the composite depending on the shape of the reinforcements, with the largest value occurring for the needle shape.

4.2 Influence of the reinforcement volume on mechanical properties of composites based on polycarbonate and polyamide matrix with glass reinforcements

The MF module and the data given in Table 5 were used to calculate the results displayed as stress-strain curves of polycarbonate composite materials filled with short, chopped glass fibers with the aspect ratio $k_r = 400$ (Fig. 10).

The material properties obtained by modeling the properties of a polycarbonate matrix composite for various glass fiber mass fractions m_f are presented in Table 5.

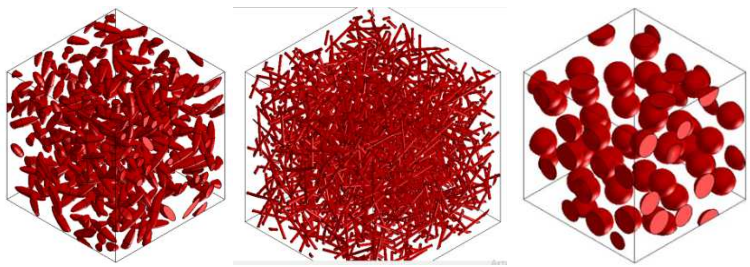

Fig. 7. Representative reinforcement elements with different proportions and shapes of inclusions. Left: ellipsoid; Center: fiber; Right: hollow glass spheres.

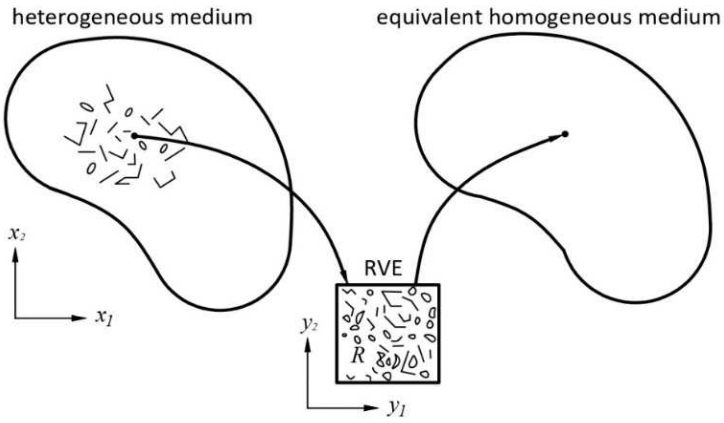

Fig. 8. Structural analysis of heterogeneous material and translation to equivalent homogenous material.

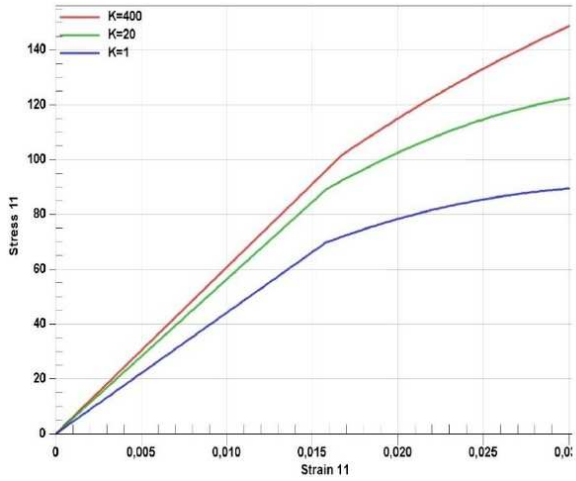

Fig. 9. Stress-strain diagrams for a polycarbonate matrix composite material with fiber reinforcement (red line); ellipsoidal reinforcements (green line); glass sphere reinforcement (blue line).

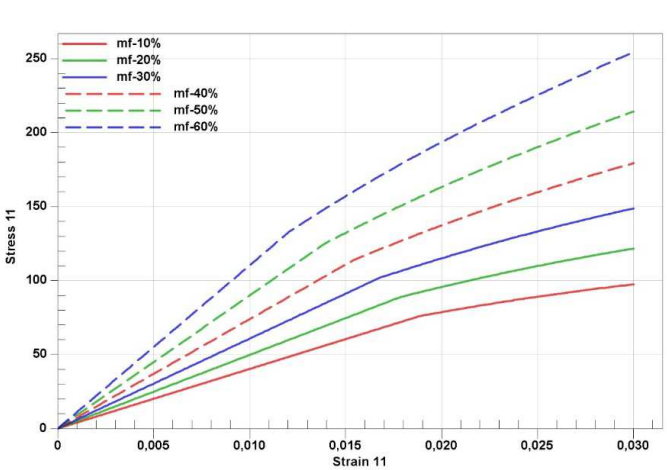

Fig. 10. Stress-strain diagrams for a polycarbonate composite material with different amounts of reinforcement: a) 10% (green line); b) 20% (red line); c) 30% (blue line); d) 40% (dashed red line); e) 50% (dashed green line); f) 60% dashed blue line.

Table 5. Calculated material parameters of glass fiber reinforced polycarbonate matrix composites.

m_f	E [MPa]	G [MPa]	ν	P [kg/mm^3]
10%	3200	1156	0.35	$1.26 \cdot 10^{-9}$
20%	4029	1498	0.33	$1.33 \cdot 10^{-9}$
30%	5060	1895	0.32	$1.415 \cdot 10^{-9}$
40%	7389	2769	0.32	$1.511 \cdot 10^{-9}$
50%	8991	3386	0.31	$1.623 \cdot 10^{-9}$
60%	11003	4175	0.31	$1.74 \cdot 10^{-9}$

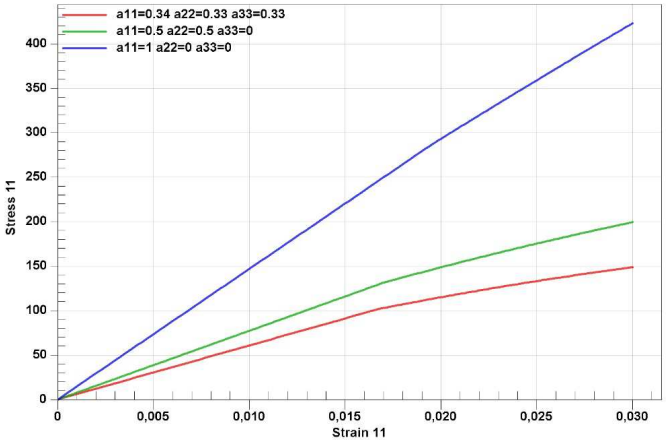

Fig. 11. Stress-strain diagrams for a polycarbonate composite material with different reinforcement orientations: a) with volumetric orientation a_{11}= 0.33, a_{22}= 0.33, and a_{33}= 0.34 (blue line); b) with flat orientation a_{11}= 0.5, a_{22}= 0.5, and a_{33}= 0 (green line); c) with flat orientation a_{11}= 0.8, a_{22}= 0.2, and a_{33}= 0 (red line).

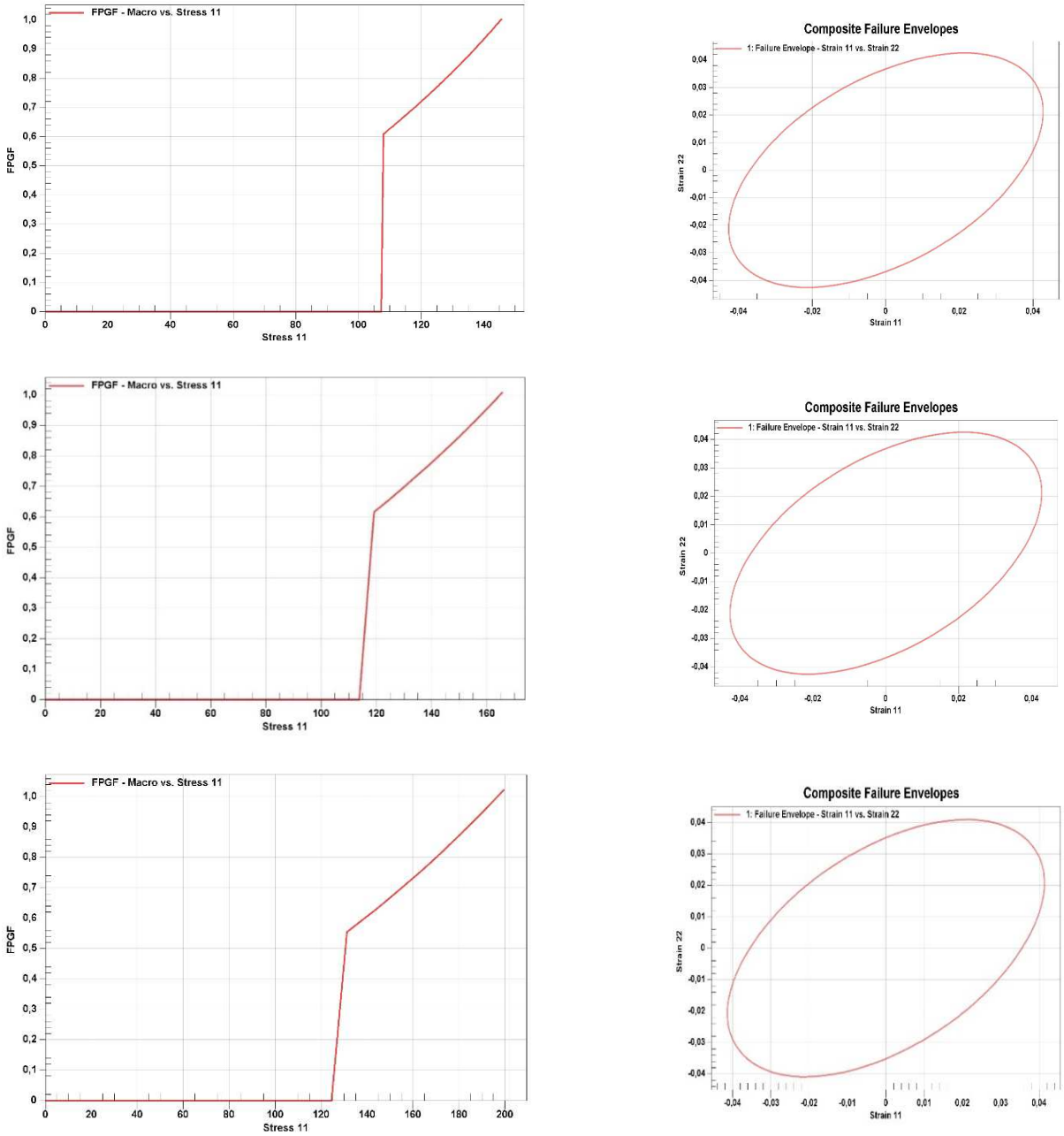

Fig. 12. Failure curves for a composite material based on a polycarbonate matrix containing: 30% reinforcement (top row); 40% reinforcement (middle row); 50% reinforcement (bottom row).

Analysis of the data presented in Table 5 indicates an increase of the modulus of elasticity and the shear modulus proportional to the increase of the mass fraction of inclusions and an appropriate decrease in the value of Poisson's ratio, indicating a loss of elasticity, and the tendency to embrittlement of the material. The density of the material also increases with an increase in the proportion of reinforcement, resulting in increased impeller mass and reduced dynamic performance of the pump rotor.

4.3 Influence of the orientation of reinforcement fibers on the mechanical properties of polycarbonate matrix composite materials

The orientation of the reinforcement fibers is one of the most significant factors affecting the mechanical properties of the composite. The indicator of this parameter is the orientation tensor T (Eq. 9):

$$T = \begin{bmatrix} a_{11} & a_{12} & a_{13} \\ a_{21} & a_{22} & a_{23} \\ a_{31} & a_{32} & a_{33} \end{bmatrix} \tag{9}$$

As there is currently no clear methodology and recommendations for creating numerical models for determining the optimal orientation of reinforcement fibers for materials based on a polycarbonate matrix and chopped glass fibers, the simulation was carried out for a flat and a volumetric layout in uniaxial direction. The stress-strain diagram presented in Figure 11 for such materials shows a large spread in the results of the mechanical characteristics of the composite, therefore it is necessary to verify the simulation results with experimental studies.

4.4 Influence of the reinforcement fiber mass fraction on the strength to failure of the composite material

Numerical simulations were run on compositions with 30%, 40%, and 50% of reinforcement since the stress-strain curves are the closest to the subject of the research, even though these curves do not reveal the ultimate strength of the material at the micro level. The failure stress values for the material were determined using the MF module with additional settings introduced according to the failure criterion.

The structural strength was predicted using the equivalent stress criteria is used, as well as the Tsai-Hill criterion for transversely isotropic bodies (3D), using the formulation of the first destroyed FPGF pseudo-grain [41].

Failure curves and strength surfaces at the micro level can be seen in Figure 12. An increase in strength with an increase in the mass fraction of the reinforcement is obvious, as a reduction in the level of strain can be seen as well. The destruction of the composite occurs at σ = 150 MPa, ε = 0.045 for 30% of the filler, σ = 165 MPa, ε = 0.045 for 40% of the filler, and σ = 150 MPa, ε = 0.04 for 50% of the filler.

5. Experimental Research of the Mechanical Material Properties of Composite Materials

According to the numerical simulations carried out at the stage of designing the properties of the composite, a polycarbonate composite material with 30% of the mass fraction of glass fiber is considered optimal to manufacture impellers. The numerical simulation made it possible to reduce the number of full-scale tests as it has revealed the most convenient method for designing new materials with desired properties.

To verify the computational data and revise the correlation of numerical data with experimental results, tests were performed using standard samples of PCM with 10%, 20%, and 30% of inclusions, that is, up to the optimal number of inclusions. Tests were performed for tension, bending, and impact strength.

5.1 Preparation of composite material

Polycarbonate matrix composites are manufactured with glass fibers chopped short. This procedure was chosen because of the molding process, as the insertion of integral fibers into the polycarbonate matrix is technologically more complicated than the manufacture of composites with short fibers. The polymer mixtures are being prepared on a single-screw Esmos extruder having 45 mm in diameter and ratio L/D = 25. The extruder is electrically heated. The temperature is controlled by thermocouples and a thermostat. The extrusion temperature regime is as follows: zone I has 260°C; zone II has 265°C; zone III has 270°C, and zone IV has 260°C.

The testing samples shown in Figure 13 were manufactured using injection molding and sized according to ISO R527.

5.2 Testing results

The tensile and flexural strength tests were carried out on a LRXplus universal testing machine. The machine is computer controlled and applies deformation with a constant strain rate. Tensile loading was carried out at the speed of 5 mm per minute. Flexural strength was measured by means of the three-point bending test. The test sample was placed as a freely supported rod loaded in the middle of the span. The load during the bending test was applied at a constant speed of 2 mm per minute. The tensile and bending test setups can be seen in Figure 14.

Fig. 13. Composite test samples: Plain matrix (left); 20% glass fiber reinforcement (center); 30% glass fiber reinforcement (right).

Fig. 14. Left: Tensile test setup; Right: Bending test setup.

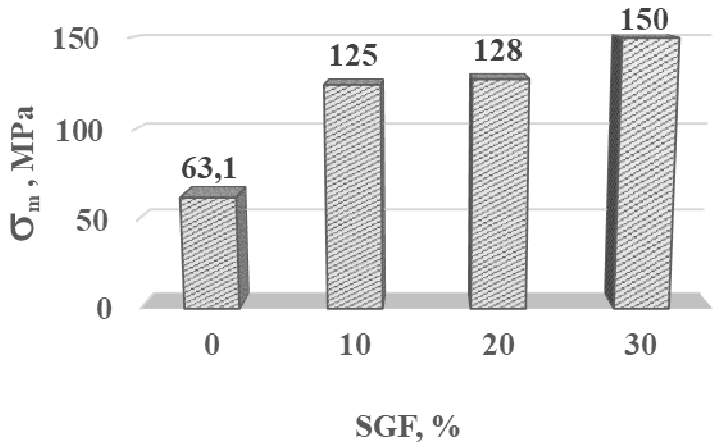

Fig. 15. Tensile strength test results.

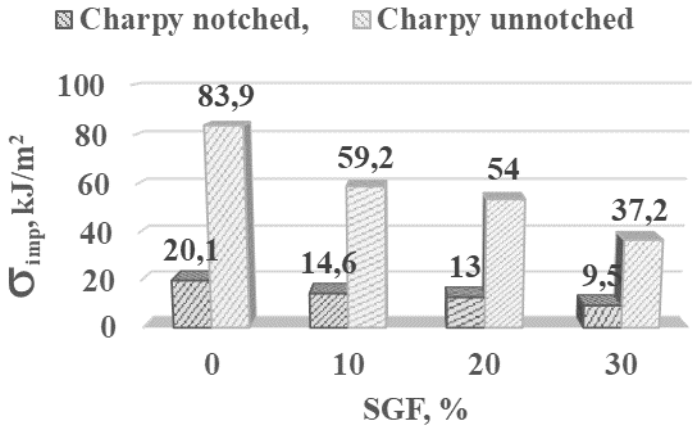

Fig. 16. Impact resistance test results.

Table 6. Experimental testing results compared to numerical simulation values.

Reinforcement ratio	0%		10%		20%		30%	
Measurement type	Experimental	Numeric	Experimental	Numeric	Experimental	Numeric	Experimental	Numeric
E_t, [MPa]	1970	(not performed)	5240	3200	5250	4029	6190	5060
σ_m, [MPa]	63.1	(not performed)	125	90	128	120	150	150

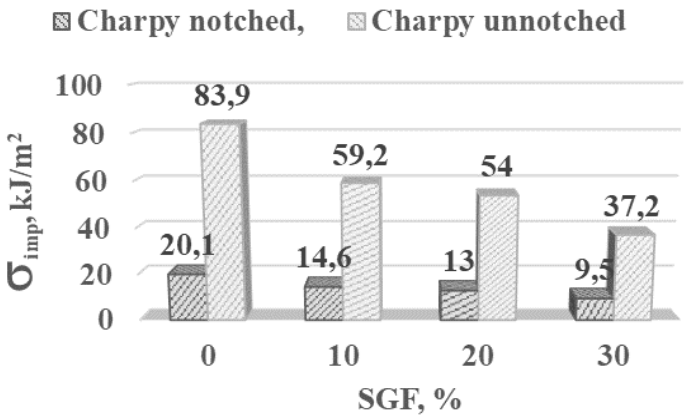

Fig. 17. Bending strength test results.

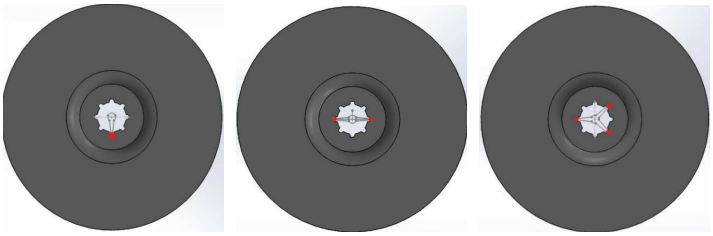

Fig. 18. Gating system installations for injection molding of PCM impellers: One injection point (left); Two injection points (center); Three injection points (right).

The results of all tests were statistically processed and charted in relation to the weight percentage of glass fiber reinforcement. Tensile strength is shown in Figure 15, impact resistance is shown in Figure 16, and bending strength is shown in Figure 17. An overview of the testing results in comparison to the results of the numerical simulation is given in Table 6.

The comparison of the results of numerical and experimental measurements shows that the average difference between the elastic modules is 30 %, while the average difference between the strength values is 7 %.

The difference between the data of numerical simulations and experimental measurements can be explained by the influence of technological factors on the strength of pump PCM details, which must be researched further.

6. Simulation of the Molding Process of a Polycarbonate Matrix Glass Reinforced Impeller

Injection molding is a four-step cyclic process of manufacturing pump details that includes the filling, packing, cooling, and ejection phases. Injection molding process parameters such as molding temperature, melt temperature, injection pressure and injection time have been introduced as important properties and cost parameters of manufactured parts [42, 43]. The optimization of this parameter for the manufacture of injected impellers has attracted the attention of many researchers.

The presence of junctions has become an important characteristic of PCM, which is now necessarily considered when creating new polymers and compositions. The nature of the influence of the technological mode of molding and the structural features of the product on the strength of the junctions depends on many factors and does not fit into simple schemes.

The development of methods for modeling three-dimensional molten flow during thermoplastic molding creates fundamentally new possibilities for predicting the flow at the flow front, and the position and properties of junctions. Computer programs for three-dimensional modeling make it easier to accurately consider influence of effects associated with melt cooling and heat dissipation in the melt near marks and edges and determine the position of junction lines on the surface of thick-walled products with complex geometry.

Computational analysis makes it possible to evaluate the influence of structural details and the gating system on the position of the junctions. Of course, it is impossible to avoid the occurrence of junctions in the presence of mesh openings in the detail, although it is possible to transfer junctions from problem areas to more advantageous ones in terms of strength and (or) appearance of the part. The most widely used software products are based on the so-called Hele-Shaw flow model, which considers a two-dimensional flow of a thermoplastic melt [44, 45]. Figure 18 shows the variation of the models of technological parameters of the gate system.

The strength of the composite material is not a conclusive value when calculated for the micro level and experimentally determined. The impeller is a complex shape which goes through an injection molding process, which in turn will also affect the final strength value of the completed detail. The degree of influence of technological factors, such as molding temperature and the number of injection points, on the strength of the finished part of the pump impeller will be determined next.

To determine the influence of technological factors, a two-factor computational experiment was planned with such factors as time, number of injection points, response - reserve factors, with the failure index (FI) (Eq. 10) calculated according to Tsai-Hill [46], while the experimental parameters matrix is listed in Table 7.

$$SF = \frac{1}{\sqrt{FI}} \tag{10}$$

The neutral levels of the factors X_1 and X_2 are temperature equal to 265°C and 2 injection points respectively.

Figure 19 shows the results of the computation in the DIGIMAT RP module, the result of the fiber strings orientation and the result of the location of the junction lines.

Table 7. Experimental parameters matrix.

Experiment number	Factor X_1	Factor X_2	Temperature X_1	Number of injection points X_2	Response y
1	1	1	270 °C	3	1.35
2	-1	1	260 °C	3	1.51
3	1	-1	270 °C	1	1.56
4	-1	-1	260 °C	1	1.49

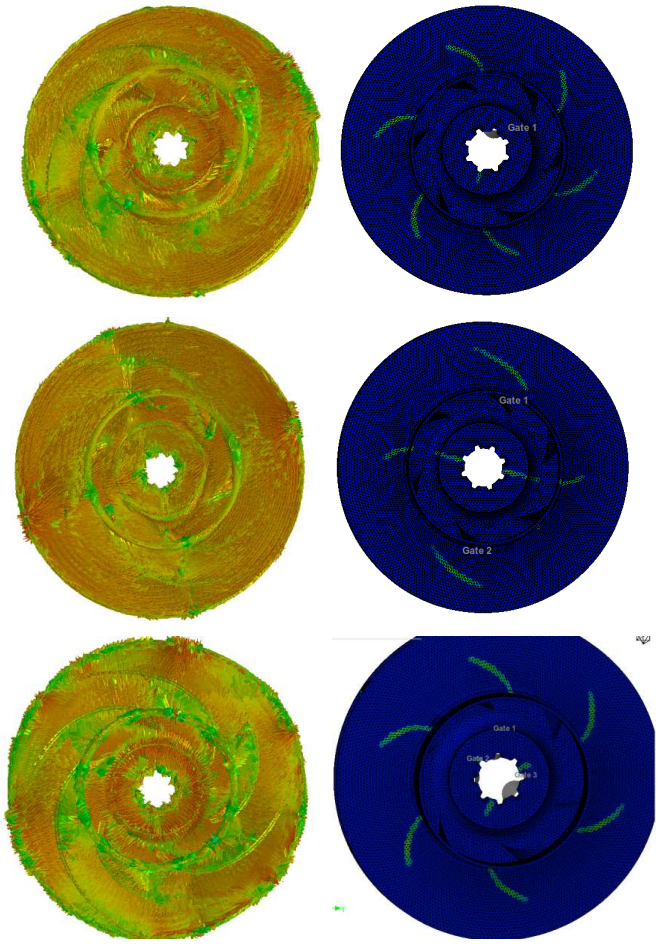

Fig. 19. Results of the analysis of the technological process and locations of the junction lines in the PMC impeller for casting: single injection point (top); two injection points (center); three injection points (bottom).

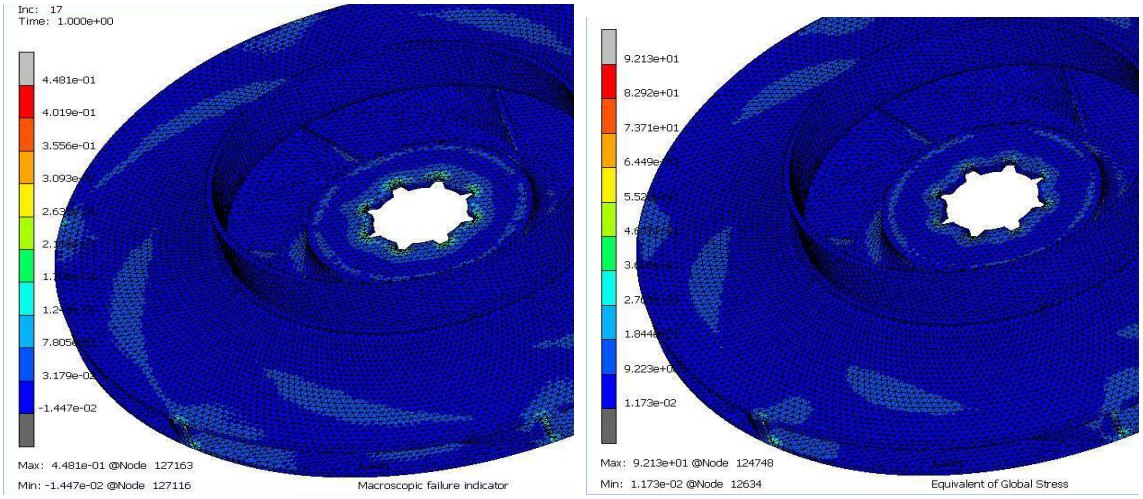

Fig. 20. The results of the stress calculation and failure criterion of PMC impeller with different options for setting injection points: Locations of highest failure probability (left); Areas of highest equivalent stress (right).

Table 8. Statistical processing of numerical results.

Experiment number	X_1	X_2	y	X_1X_2	X_2^2	$X_2^2X_2^2$	$X_1X_2^3$	X_1X_2y	X_2^4	X_2^2y
1	270	3	1.41	810	9	656100	7290	1142.1	81	12.69
2	260	3	1.51	780	9	608400	7020	1177.8	81	13.59
3	270	1	1.56	270	1	72900	270	421.2	1	1.56
4	260	1	1.49	260	1	67600	260	387.4	1	1.49
Σ	1060	8	5.97	2120	20	1405000	14840	3128.5	164	29.33

It can be noted in the diagrams shown in Figure 20, that junction lines are formed at the places where the orientation of the fiber strings changes. It is also necessary to note the location of the junction lines, as stress concentration occurs at the junction lines, mesh openings and mounting positions. The numerical calculation shows that the highest intensity of stress concentration occurs with two injection points along two long junction lines.

The integration of the DIGIMAT RP and MARC MENTAT systems made it possible to carry out the calculation considering the physical nonlinearity of the model and determine the maximum stresses that occur at the cross-sections of the impeller made of composite material, as well as determining the detail failure criterion. The results are shown in Figure 20.

The results of the numerical experiments according to the matrix of the experiment are included in Table 8 of the regression analysis. The response of the system to technological factors was determined by regression analysis and a regression equation of the following form (Eq. 11):

$$\hat{y} = b_0 + b_{12}x_1x_2 + b_2x_2^2 \tag{11}$$

The relation equation is obtained after solving the system of linear equations and determining the regression coefficients (Eq. 12):

$$\hat{y} = 1.99025 + 0.0023x_1x_2 + 0.14425x_2^2 \tag{12}$$

The strength function response surface in relation to the technological factors of temperature and the number of injection points is shown in Figure 21. To analyze the extremum of the function values, we take only an integer number of factor values X_2. This means that the maximum value of the strength factor under the condition of energy saving will be achieved at three injection points, and a slight improvement in strength quality by 0.005% will be achieved by increasing the process temperature by 10°C and a decrease in injection points to 1. The extremum of the function - the minimum strength is reached at the point corresponding to two injection points and a temperature of 270°C.

7. Conclusion

The detailed methodology for numerical simulation of a composite material based on polycarbonate with chopped fibers to produce impellers of a multistage pump was presented in this article. Numerical analysis was performed to determine the stress-strain curve and the failure criterion at the microlevel, making it possible to predict the strength of the composite and reduce the number of full-scale experiments. The results of numerical analysis and full-scale experiments decided the composition of polycarbonate and chopped fibers. The tensile strength of the material reaches 150 MPa, with the difference between numerical and full-scale experiments occurred as 7% in stress-strain and 20% in engineering data, the difference being conditioned by the influence of technological factors of the injection molding process.

The modeling of the process of centrifugal pump impeller molding from a glass polymer made it possible to draw the conclusion that junction lines are formed in places where the orientation of the fiber strings changes. It is also necessary to note the location of the junction lines, as most stress concentration occurs at the junction lines at the mesh openings and at the mounting positions. The numerical experiment also shows that the most stress concentration occurs with two injection points, resulting in two long junction lines.

According to the results of the two-factor numerical analysis for the determination of the influence of the process temperature and the number of injection points in the gating system, an equation was derived for the relation of the composite material strength on the parameters of the technological process, according to the extrema of the response function. It was found that the most optimal parameters in terms of energy saving, and strength of the molded impeller detail occurred as a combination of three injection points at a temperature of 260°C, while the minimum strength was reached with two injection points at a temperature of 270°C.

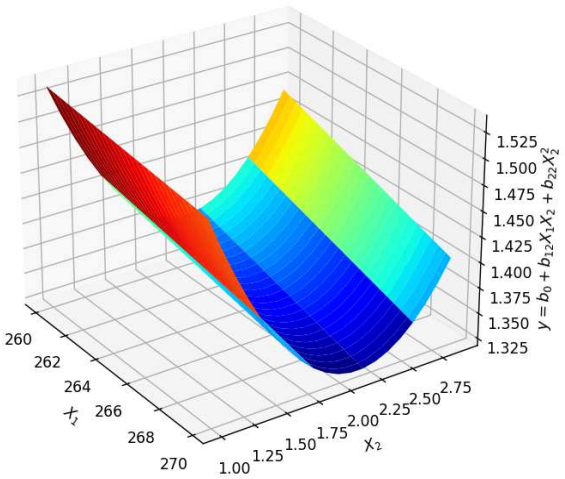

Fig. 21. Strength function response surface.

Author Contributions

M. Isametova initiated the project and conducted computer modeling of the mechanical characteristics of the composite. R. Nussipali performed numerical analysis on the strength of impeller wheels. D. Karaivanov conducted part of the research related to the physical experiment and planned the experiment. Z. Abilikhair conducted a review of the literature and an overview of the state of art. A. Isametov calculated the dimensions of the wheel in PYTHON and carried out flow simulations. The manuscript was written by the contribution of all the authors. All the authors discussed the results, reviewed, and approved the final version of the manuscript.

Acknowledgments

The authors would like to express their gratitude to the editor and to the reviewers for their encouraging comments and assistance in improving the manuscript.

Conflict of Interest

The authors declare that there are no potential conflicts of interest concerning the research, authorship, and publication of this article.

Funding

This work was supported by the Ministry of Education and Science of the Republic of Kazakhstan through project AP08857367 “Development of innovative technologies for improving energy efficiency and reliability of centrifugal pumps manufactured in Kazakhstan”, for which the authors are very grateful.

Data Availability Statements

The datasets generated and/or analyzed during the current study are available from the corresponding author on reasonable request.

Nomenclature

Q_H	Nominal pump volumetric flow [m^3/h]	ν	Poisson’s ratio [-]
H_H	Pump head [m]	σ_{max}	Maximum stress [MPa]
n_h	Rotational velocity [min^{-1}]	y	Displacement [mm]
t	Temperature [°C]	m_f	Mass fraction of inclusions [%]
ρ	Density [kg/m^3]	a_{ij}	Orientation tensor component
p	Pressure [MPa]	σ_m	Strength limit [MPa]
w	Absolute velocity [m/s]	SF	Safety factor [-]
E	Modulus of elasticity [MPa]	FI	Failure index [-]
G	Shear modulus [MPa]	ε	Strain [-]

References

[1] Yakimov, S.B., Ivanovsky, V.N., Degovtsov, A.V., Eliseev, D.B., Aygishev E.V., On the Influence of the Fraction Composition of Abrasive Particles in Produced Fluid on the Wear Types of the Elements of Electric Centrifugal Pumps, *Territorija Neftegas [Oil and Gas Territory]*, 11, 2017, 32-38.
[2] Fragassa, C., Lightening structures by metal replacement: from traditional gym equipment to an advanced fiber-reinforced composite exoskeleton, *Facta Universitatis-Series Mechanical Engineering*, 19(2), 2021, 155–174.
[3] Tserpes, K., Tzatzadakis, V., Computation of mechanical, thermal, and electrical properties of CNT/polymer multifunctional nanocomposites using numerical and analytical models, *MATEC Web of Conferences*, 304, 2019.
[4] Mastrogiannakis, I., Vosniakos, G., Exploring structural design of the Francis hydro-turbine blades using composite materials, *Facta Universitatis-Series Mechanical Engineering*, 18(1), 2020, 43-55.
[5] Zirak, N., Shirinbayan, M., Deligant, M., Tcharkhtchi, A., Toward Polymeric and Polymer Composites Impeller Fabrication. *Polymers,* 14, 2022, 97.
[6] Wang, R., Zheng, S., Zheng, Y., *Polymer matrix composites and technology*, Woodhead Publishing, Cambridge, 2011.
[7] Ahmadifar, A., Zamani, M.R., Davar, A., Jam, J.E., Beni, M.H., Experimental and Numerical Buckling Analysis of Carbon Fiber Composite Lattice Conical Structure before and after Lateral Impact, *Journal of Applied and Computational Mechanics*, 6, 2020, 813-822.
[8] Mallick, Vi., Thermoplastic composite based processing technologies for high performance turbomachinery components, *Composites Part A-Applied Science and Manufacturing*, 32, 2001,1167-1173.
[9] Li, Q., Piechna, J., Müller, N., Static, Dynamic and Failure Behavior of a Novel Axial Composite Impeller for Water Chiller, *ASME International Mechanical Engineering Congress and Exposition, Proceedings (IMECE)*, 36(5), 2010, 2773-2781.
[10] Pavlovic A., Finite Elements Analysis of the Hyperelastic Impeller Rotating in the Self-Priming Pump, *Journal of Applied and Computational Mechanics*, 8(3), 2022, 1103-1112.
[11] Islam, M.N., Ar-Rashid, H., Islam, F., Karmaker, N., Koly, F.A., Mahmud, J., Keya, K., Khan, R., Fabrication and Characterization of E-Glass Fiber Reinforced Unsaturated Polyester Resin Based Composite Materials, *Nano Hybrids and Composites*, 24, 2019, 1-7.
[12] Liu, Y., Guo, Y., Zhao, J., Chen, X., Zhang, H., Hu, G., Yu, X., Zhang, Z., Carbon fiber reinforced shape memory epoxy composites with superior mechanical performances, *Composites Science and Technology*, 177, 2019, 49–56.
[13] Nayak, R.K., Ray, B.C., Rout, D., Mahato, K.K., *Hydrothermal Behavior of Fiber- and Nanomaterial-Reinforced Polymer Composites (1st Ed.)*, CRC Press, Boca Raton, 2020.
[14] Mohan, N., Mahesha, C., Rajaprakash, B.M., Erosive Wear Behaviour of WC Filled Glass Epoxy Composites, *Procedia Engineering*, 68, 2013, 694-702.
[15] Öztürk, B., Gedikli, H., Kılıçarslan, Y.S., Erosive wear characteristics of E-glass fiber reinforced silica fume and zinc oxide-filled epoxy resin composites, *Polymer Composites*, 41(1), 2019, 326-337.
[16] Zirak, N., Shirinbayan, M., Deligant, M., Tcharkhtchi, A., Toward Polymeric and Polymer Composites Impeller Fabrication, *Polymers*, 14(1), 2021, 1-25.
[17] Gülich, J.F., Effect of Reynolds number and surface roughness on the efficiency of centrifugal pumps, *Journal of Fluids Engineering*, 125, 2003, 670–679.
[18] Elanchezhian, C., Ramnath, B.V., Hemalatha, J., Mechanical Behaviour of Glass and Carbon Fibre Reinforced Composites at Varying Strain Rates and Temperatures, *Procedia Materials Science*, 6, 2014, 1405-1418.
[19] Marius, S., On the durability of progressive cavities pumps, *Reliability & Durability*, 1, 2018, 187–192.
[20] Kostyuk, A.G., *Dinamika i prochnost’ turbomashin*, Izdatel’skiy dom MEI, Moscow, 2007.

[21] Roche-Carrier, N.L., Ngoma, G.D., Ghié, W., Numerical Investigation of a First Stage of a Multistage Centrifugal Pump: Impeller, Diffuser with Return Vanes, and Casing, *International Scholarly Research Notices*, 2013, 2013, 1-15.
[22] Spasic, Ž., Jovanovic, M., Bogdanovic-Jovanovic, J., Milanovic, S., Numerical investigation of the influence of the doubly curved blade profiles on the reversible axial fan characteristics, *Facta Universitatis-Series Mechanical Engineering*, 18(1), 2020, 057-068.
[23] Zhang, Z.C., Wang, F.J., Yao, Z.F., Leng, H.F., Zhou, P.J., Investigation on impeller radial force for double-suction centrifugal pump with staggered blade arrangement, *IOP Conference Series: Materials Science and Engineering*, 52(3), 2013, 032009.
[24] Nadal, E., Ródenas, J.J., Albelda, J., Tur, M., Tarancón, J.E., Fuenmayor, F.J., Efficient finite element methodology based on cartesian grids: application to structural shape op1timization, *Abstract and Applied Analysis*, 2013, 2013, 1-19.
[25] Isaeva, I., Povetkin, V., Isametova, M., Kerimzhanova, M., Bukayeva, A., Ibragimova, Z., Assessment of dynamic parameters of heavy-duty gears, *Vibroengineering Procedia*, 10, 2016, 46-51.
[26] Zhu, S., Guo, Y., Chen, Y., Liu, S., Low Water Absorption, High-Strength Polyamide 6 Composites Blended with Sustainable Bamboo-Based Biochar, *Nanomaterials*, 10(7), 2020, 1-15.
[27] Suzuki, T., Chihara, H., Kotaka, T., Sorption of Water by Bisphenol-A Polycarbonate and Polyoxyethylene Multiblock Copolymers with Varying Composition and Block Length, *Polymer Journal*, 16, 1984, 129-138.
[28] Nazarov, S.A., Teorema Eshelbi i zadacha ob optimalnoi zaplate, *Algebra i Analiz*, 21(5), 2009, 155–195.
[29] Barral, M., Chatzigeorgiou, G., Meraghni, F., Leon, R., Homogenization using modified Mori-Tanaka and TFA framework for elastoplastic-viscoelastic-viscoplastic composites: Theory and numerical validation, *International Journal of Plasticity*, 127, 2020, 102632.
[30] McCarthy, C.T., McCarthy, M.A., Gilchrist, M.D., Predicting Failure in Multi-Bolt Composite Joints Using Finite Element Analysis and Bearing-Bypass Diagrams, *Key Engineering Materials*, 293-294, 2005, 591-598.
[31] Osman, M.A., Atallah, A.S., Effect of the particle size on the viscoelastic properties of filled polyethylene, *Polymers*, 47, 2006, 2357-2368.
[32] Yang, K., Yang, Q., Li, G., Sun, Y., Feng, D., Mechanical properties and morphologies of polypropylene with different sizes of calcium carbonate particles, *Polymer Composites*, 27, 2006, 443-450.
[33] Ozawa, Y., Watanabe, M., Kikuchi, T., Ishiwatari, H., Mechanical and thermal properties of composite material system reinforced with micro glass balloons, *IOP Conference Series: Materials Science and Engineering*, 10(1), 2010, 012094.
[34] Saba, N., Safwan, A., Sanyang, M.L., Mohammad, F., Pervaiz, M., Jawaid, M., Alothman, O.Y., Sain, M.M., Thermal and dynamic mechanical properties of cellulose nanofibers reinforced epoxy composites, *International Journal of Biological Macromolecules*, 102, 2017, 822-828.
[35] Singh, U.P., Biswas, B.K., Ray, B.C., Evaluation of mechanical properties of polypropylene filled with wollastonite and silicon rubber, *Materials Science and Engineering:* A, 501(1-2), 2009, 94–98.
[36] Bazhenov, S., Serenko, O., Dubnikova, I., Berlin, A., Criterion of the Appearance of Diamond-Shaped Pores in Dispersely Filled Polymers, *Doklady Physics*, 48, 2003, 640-643.
[37] Dubnikova, I.L., Kedrina, N.F., Solov'eva, A.B., Timofeeva, V.A., Rozhkova, N.N., Erina, N.A., Zarkhina, T.S., The effect of filler nature on the crystallization behavior and mechanical properties of filled polypropylene, *Polymer Science: Series A, Chemistry, Physics*, 45, 2003, 281-286.
[38] Krairi, A., Doghri, I., Multi-scale Damage Model for Mechanical High Cycle Fatigue (HCF) of Short Glass Fibre Reinforced Thermoplastics (SGFRTP), *Procedia Engineering*, 66, 2013, 759-765.
[39] Isametova, M., Abilezova, G., Dishovsky, N., Velev, P., Development and verification of mechanical characteristics of a composite material made of a thermoplastic matrix and short glass fibers, *Eastern-European Journal of Enterprise Technologies*, 5, 2021, 30-38.
[40] Fernandes, C., Pontes, A.J., Viana, J.C., Gaspar-Cunha, A., Modeling and optimization of the injection-molding process: a review, *Advances in Polymer Technology*, 37, 2018, 429-449.
[41] Rosli, M.U., Termizi, S.N.A.A., Khor, C.Y., Nawi, M.A.M., Omar, A.A., Ishak, M.I., *Optimisation of Process Parameters in Plastic Injection Moulding Simulation for Blower Impeller's Fan Using Response Surface Methodology*, In: Intelligent Manufacturing and Mechatronics, Springer, Singapore, 2021, 309–318.
[42] Khan, M., Afaq, S.K., Khan, N.U., Ahmad, S., Cycle Time Reduction in Injection Molding Process by Selection of Robust Cooling Channel Design, *International Scholarly Research Notices*, 2014, 1-8.
[43] Mashkov, Iu. K., Mekhanicheskie i tribotekhnicheskie svoistva polimernykh kompozitsionnykh materialov na osnove PTFE, optimizatsiia ikh sostava i tekhnologii, *Vestnik SibADI*, 4(18), 2010, 17–21.
[44] Fernandes, C., Pontes, A.J., Viana, J.C., Gaspar-Cunha, A., Modeling and optimization of the injection-molding process: a review, *Advances in Polymer Technology*, 37, 2018, 429-449.
[45] Bociaga, E., Jaruga, T., Lubczynska, K., Gnatowski, A., Warpage of injection moulded parts as the result of mould temperature difference, *Archives of Materials Science and Engineering*, 44, 2010, 28-34.
[46] Choudhury, A., Mondal, S.C., Sarkar, S., Failure Analysis of Laminated Composite Plate Under Hygro-Thermo Mechanical Load and Optimisation, *International Journal of Applied Mechanics and Engineering*, 24, 2019, 509-526.

ORCID iD

Madina Isametova https://orcid.org/0000-0003-4630-271X
Rollan Nussipali https://orcid.org/0000-0001-6965-0667
Dimitar Karaivanov https://orcid.org/0000-0002-1709-677X
Zhastalap Abilikhair https://orcid.org/0000-0002-7568-1061
Aysen Isametov https://orcid.org/0000-0003-1036-2294

How to cite this article: Isametova M., Nussipali R., Karaivanov D., Abilikhair Z., Isametov A. Computational and Experimental Study of the Composite Material for the Centrifugal Pump Impellers Manufacturing, *J. Appl. Comput. Mech.*, 8(4), 2022, 1407–1421. https://doi.org/10.22055/jacm.2022.40366.3574